AIAA-2001-0302

Flow-Tagging Velocimetry for Hypersonic Flows Using Fluorescence of Nitric Oxide

P.M. Danehy
Instrumentation Systems Development Branch
NASA Langley Research Center
Hampton, VA, USA

S. O'Byrne, A.F.P. Houwing
Physics Department
Australian National University
Canberra, ACT, Australia

39th AIAA Aerospace Sciences Meeting and Exhibit
8-11 January 2001 / Reno, NV

Flow-tagging velocimetry for hypersonic flows using fluorescence of nitric oxide

P. M. Danehy*,
Instrumentation Systems Development Branch
NASA Langley Research Center, Hampton, VA, USA

S. O'Byrne†, A.F.P. Houwing‡
Department of Physics, Faculty of Science
Australian National University, Canberra, ACT, AUSTRALIA

Abstract

We investigate a new type of flow-tagging velocimetry technique for hypersonic flows. The technique involves exciting a thin line of nitric oxide molecules with a laser beam and then, after some delay, acquiring an image of the displaced line. One component of velocity is determined from the time of flight. This method is applied to measure the velocity profile in a Mach 8.5 laminar, hypersonic boundary layer in the Australian National University's T2 free-piston shock tunnel. The velocity is measured with an uncertainty of approximately 2%. Comparison with a CFD simulation of the flow shows reasonable agreement.

Introduction

Velocity is one of the most important flowfield parameters to measure in non-reacting flows. The velocity field is particularly important in hypersonic flows because it describes the distribution of kinetic energy within the flow. While several very good methods for measuring velocity in hypersonic flows exist, this paper describes a new flow-tagging method that should be particularly convenient to use in certain specialized flow facilities.

We use this new method to measure the velocity profile of the laminar boundary layer that develops on a flat plate placed in a hypersonic freestream. This flow has been studied extensively both computationally and experimentally. Good agreement has been found between predicted and measured pressure and heat transfer distributions.[1,2] However, because of the difficulty in accurately measuring flowfield parameters in hypersonic facilities, satisfactory agreement between predicted and measured density[1,2], temperature[3], and velocity[1] profiles within the boundary layer have not yet been realized to our knowledge.

The goal of the present experiment was to develop a method suitable for measuring the velocity in this flowfield; this velocity profile could then be compared with theoretical models that predict the flow, in an effort to validate these models. This experiment is part of a larger study of laminar hypersonic boundary layers, including heat transfer measurements and planar laser-induced fluorescence (PLIF) temperature measurements that will be presented elsewhere.[4]

Velocity has been measured in high-speed gas flows using a variety of different methods. Hypersonic flowfields are a challenging environment for many velocimetry techniques, for a variety of reasons. Physical probes such as hot-wire anemometers are inappropriate for studying supersonic or hypersonic flows since they disturb the flow and because their size limits the spatial precision of the measurements. In shock tunnels, line-imaging or two-dimensional imaging methods are preferred to single-point methods such as laser Doppler velocimetry (LDV) or laser-induced thermal acoustics (LITA)[5] because the limited test time of the flow makes it very expensive to map the velocity field.

Several laser-based methods have been developed for mapping the velocity in gaseous flows. These include particle image velocimetry (PIV) and planar Doppler velocimetry (PDV)[6,7]. Both of these methods rely on scattering of light from particles present or seeded in the flow. In hypersonic flows, particles do not always follow the flow. Also, in impulse facilities like shock tunnels, it is difficult to seed particles uniformly into the flow. For this reason, methods involving scattering from molecules present in the flow are more desirable. Rayleigh scattering velocimetry[8,9,10] and planar laser-induced fluorescence (PLIF) velocimetry are two widely used molecular based methods. Both of these methods use the Doppler shift of the scattered light to determine the flow velocity. We found that Rayleigh scattering velocimetry could not be used in the Australian National University's free piston shock tunnels because Mie scattering (from particles) overwhelmed Rayleigh scattering (from molecules) by more than an order of magnitude. A molecular absorption filter is commonly

---

* Scientist, Member AIAA
† Graduate Student, Student Member AIAA
‡ Senior Lecturer, Member AIAA

used to separate Mie and Rayleigh signals. However, we could not use an absorption filter because in the present experiment both particles and molecules were moving at hypersonic velocities in some parts of the flow, and subsonic velocities elsewhere. Without a way to separate the Mie and Rayleigh signals in this flow, we abandoned that approach in favour of PLIF velocimetry. PLIF signal is spectrally separate from laser scatter and therefore the elastic scattering from particles and surfaces can be filtered out. We have recently had success using PLIF to measure the radial component of velocity in ANU's T2 free-piston shock tunnel.[11] Doppler-based PLIF velocimetry has previously been used to measure 2 components of velocity by several authors.[12,13,14] However, because of the optical access limitations in ANU's shock tunnels, another method for measuring the streamwise velocity was sought.

PLIF has been used in a wide variety of velocimetry methods based on flow tagging.[15,16,17,18,19] In these methods, time-of-flight of laser-excited molecules is used to determine the flow velocity. Unfortunately all of these flow-tagging methods except Ref. 19 require two or three independently tuneable and delayable pulsed lasers. One laser is typically used to write a line into the flow (via Raman excitation, dissociation, or ionisation) and the second laser is used to probe the displacement of this line at a subsequent time. Hiller et al.[19] developed a flow-tagging velocimetry method requiring only a single pulsed laser. They demonstrated the technique by seeding the molecule Biacetyl into a subsonic flow and observing its phosphorescence after laser excitation. However, Hiller et al.'s method has seldom been used since.

Our paper extends the method of Hiller et al.[19] to a new molecule and to high-speed flows. The technique is illustrated schematically in Figure 1. We used a tuneable pulsed laser to excite a thin line of nitric oxide (NO) molecules which are naturally present in the shock-tunnel flow. These excited molecules fluoresce as they convect downstream. If the flow velocity is high and the test gas composition is chosen to have a low collisional quenching rate, Q, then the fluorescence will continue over a short distance, eg. a few millimeters. By introducing a delay between the laser excitation pulse and the camera acquisition time, one can observe the downstream movement of the tagged molecules, from which the velocity can be simply calculated.

This method has several advantages compared to other velocimetry methods. First, it uses a single laser which reduces cost and set-up time. Second, this method is very convenient in many laboratories, like ours, where scientists are already performing PLIF thermometry: one needs only to adjust the two sheet forming lenses (described in detail below) and delay the camera acquisition time to measure the velocity. Third, the method is conceptually simple with few required assumptions and therefore the data obtained should be reliable. Fourth, the analysis of the raw data to obtain velocity is straight-forward. Fifth, the method can measure velocity along a line in the flow during a single laser pulse, and it can be extended to measure additional

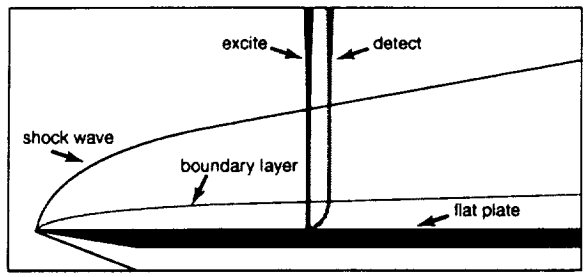

Figure 1 Schematic of LIF flow tagging of the boundary layer on a flat plate. Flow is from left to right.

velocity components in a straightforward manner. Finally, the method uses much lower pulse energy (~1 mJ) compared to many other flow tagging methods (eg, RELIEF[16] typically uses hundreds of milliJoules to tag the molecules), so likelihood of damage to expensive aerospace vehicle models is reduced, as are systematic errors due to surface heating from the incident radiation. The most notable disadvantage of the method is that the flow velocity, u, must be greater than w/τ_{LIF} where w is the laser sheet width and τ_{LIF} is the fluorecence lifetime. This limitation limits the applicability of this method to high-velocity, low collisional quenching flow environments.

Theory

A. Fluorescence Tagging Velocimetry Method

The PLIF method has been used extensively to study combustion and also in fluid mechanics (see references 20 and 21 and references therein). PLIF uses a laser to promote molecules from their ground states to excited states. Once in the excited state, the molecules fluoresce. This fluorescence is captured by a digital camera. The theory of PLIF is well understood. Many PLIF measurement techniques (thermometry, Doppler-based velocimetry, mole fraction imaging, etc.), require a detailed understanding of the PLIF excitation and fluorescence process, including the accurate knowledge of the absorbing molecules' spectroscopy and energy transfer rates. However, the present method only depends on one critical parameter: the fluorescence lifetime, $\tau_{LIF} = 1/(A+Q)$ where A is the spontaneous emission rate and Q is the collisional quenching (de-excitation) rate. Assuming that the laser pulse duration, τ_L, is much shorter than τ_{LIF}, the time evolution of the fluorescence intensity is given by:

$$I_{LIF} = I_{LIFo} \exp(-t/\tau_{LIF}) \qquad (1)$$

where I_{LIFo} is the fluorescence intensity at the end of the laser pulse (ie., the start of the exponential decay).

Nitric oxide laser-induced fluorescence is a particularly appropriate optical measurement scheme for use in shock tunnels. NO is generated naturally by the shock-heating process during normal operation which means that toxic gas handling systems are not required to seed NO into the flow. Furthermore, the NO mole

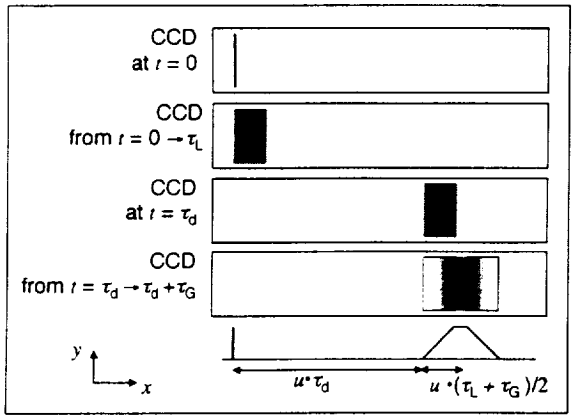

Figure 2 Schematic of images that would be acquired by a CCD camera at different delays and gate durations during the experiment.

fraction can be adjusted between 0 and ~8% by varying the ratio of O_2/N_2 in the shock tube gas.

For the first excited electronic state of NO which is populated by the laser in this experiment, A has been measured to be ~1/(220 ns).[22] Thus, in the absence of quenching collisions, $\tau_{LIF} = 220$ ns. Increasing Q always reduces the fluorescence lifetime. Paul et al.[22] provide rate constants and formulae for computing the collisional quenching rates for NO when colliding with other species. Of interest in the current work: O_2 quenches NO fluorescence over 3 orders of magnitude more efficiently than N_2. For fluorescence flow tagging velocimetry, we can improve the signal-to-noise ratio of the acquired images by mimimizing Q, thereby maximizing τ_{LIF} so that the fluorescence is long lived. The longer the fluorescence lasts, the longer the delay that can be used between the laser and camera, and the more sensitive the velocity measurement.

Once the delayed fluorescence images are acquired, they must be processed to determine the displacement of the tagged gas. We have used an algorithm provided by Dr. Glenn Diskin from NASA Langley Research Center, Hampton, VA, USA. The algorithm first smooths the raw data by convolving the raw image with a 3 pixel by 4 pixel wide Gaussian function (oriented so that there is less smoothing in the streamwise direction). Next, the maximum intensity along each row of the image (in the streamwise direction) is determined. Finally, a quadratic polynomial is fit to the three pixels nearest the maximum along that row to determine the center of the displaced line. This process is repeated for each row in the image to determine displacement as a function of height above the flat plate.

If the laser sheet is not oriented perpendicular to the flow, then the method described above can lead to a systematic error in the measured velocity. To account for this laser-sheet misalignment, we obtain a fluorescence image prior to each shot in the tunnel by filling the test chamber with static gas containing a small amount of NO. This image is analysed at the same time as the delayed flowfield images and the static gas measurement is subtracted from the flow measurement to correct for laser-sheet misalignment.

In general, time-of-flight velocity is determined from:

$$u = \frac{d}{\tau_d} \qquad (2)$$

where u is the flow velocity, d is the displacement measured from the images, and τ_d is the delay between the laser pulse and the camera acquisition. However, this is only true in the limit that the laser pulse duration, τ_L, and the camera gate duration, τ_G, are negligible compared to τ_d. In the current experiment, τ_d varies from 250 ns to 750 ns, whereas τ_L is 20±3 ns and τ_G is 30±3 ns. Thus, these durations are significant, and need to be considered in the present work.

Figure 2 shows a schematic that explains how we determined the appropriate delay time to use in the analysis. For the purpose of this analysis, we shall assume that the laser sheet is infinitely thin and we will neglect the fact that the intensity of the fluorescence is decaying exponentially during the experiment. The first assumption is exactly valid: the finite width of the laser sheet does not introduce a systematic error into the measurement. The finite width does, however, reduce the sensitivity of the measurement. The second assumption is not particularly good: the LIF intensity does decay slightly during the measurement time. If the tagged line was infinitely narrow, this would cause the fluorescence to decrease with distance in the acquired image. The fitting algorithm described above would then produce a systematically inaccurate velocity. However, in the present experiment, the tagged line has a finite width of ~6.5 pixels. Considering that the images are smoothed before processing and that the flow moves less than 2 pixels during the acquisition time, we estimate the systematic error from this effect to be small compared to other errors in the experiment. In this analysis, we also assume that the laser pulse and camera gate each have top-hat temporal profiles. Futhermore, we neglect thermal diffusion.

Figure 2 shows the fluorescence image that would be obtained at various times in the experiment. The top panel (CCD at $t = 0$), shows how the fluorescence image would look just after the laser turned on, assuming that the camera gate duration was infinitesimal (say <1 ns). The second panel (CCD from $t = 0 \rightarrow \tau_L$) shows the image that would be obtained if the camera gate opens at time zero and remains open for a duration equal to τ_L. In this case, the gas moves during the time that the laser is on. So, the laser tags a patch of gas with a spatial width equal to $u \cdot \tau_L$. Note that if the velocity is equal to zero (as it is in the static gas measurement performed as a reference, prior to each shot) then the width of this patch of gas is infinitesimal and the image looks identical to the top panel.

The third panel (CCD at $t = \tau_d$) shows how the tagged gas would look if imaged by a camera delayed by τ_d, and having an infinitely short gate duration. This image shows that the tagged patch of gas has translated by a distance equal to $u \cdot \tau_d$. The fourth panel (CCD from $t = \tau_d \rightarrow \tau_d + \tau_G$) shows the image that would be acquired by a camera gate that is delayed from the laser pulse by τ_d

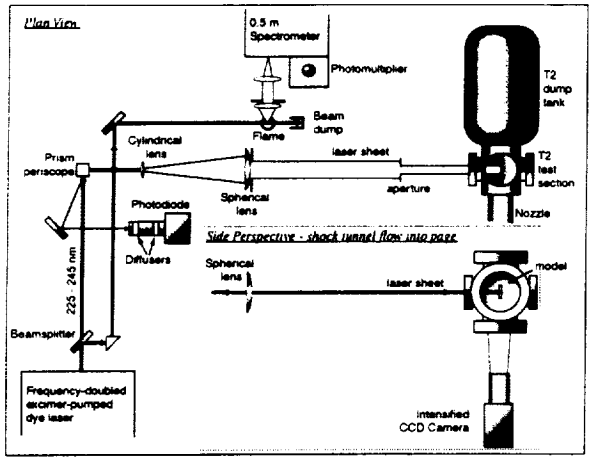

Figure 3 Schematic of the experiment. In the present experiment, the cylindrical lens was rotated by 90 degrees to orient the laser sheet across the span of the flat plate. An aperture in front of the test section clipped the beam to a width of 3 mm.

and that has a duration of τ_G. In this case, the image is a convolution of the tagged patch of gas and the camera gate. The center of this trapezoidal area is displaced to the right of the left edge of the trapezoid by the distance equal to $u\bullet(\tau_L+\tau_G)/2$. This motional blurring does occur in the experiment, though in the figure it is greatly exaggerated for clarity.

In the experiment and image analysis, we determine the displacement, d, between the static gas (an image similar to the top panel) and the image acquired during the shot (an image similar to the fourth panel). Thus, the velocity is computed according to:

$$u = \frac{d}{\tau_d + (\tau_L + \tau_G)/2} \qquad (3)$$

B. Hypersonic Boundary Layer Flow

The laminar boundary layer that forms on a flat plate in a hypersonic flow is a relatively well-understood flowfield.[1,2] As shown in Figure 1, a thin boundary layer grows on the flat plate. The boundary layer grows quadratically near the leading edge, and linearly further downstream. The rapid growth of the boundary layer at the sharp leading edge causes a weak shock wave to form. This shock weakens as it bends downstream, as shown in the figure. One of the characteristics that distinguish hypersonic boundary layers from their supersonic and subsonic counterparts is that the temperature in the boundary layer increases dramatically above the freestream temperature in the middle of a hypersonic boundary layer as viscosity converts kinetic energy to thermal energy. If the wall is not insulated, then the temperature in the boundary layer adjacent to the wall approaches the wall temperature.

A slight complication in the present experiment is that we used a conical nozzle. Thus, the flow continues to diverge as it passes along the flat plate. This causes a slight pressure gradient in the freestream that must be accounted for in the CFD.

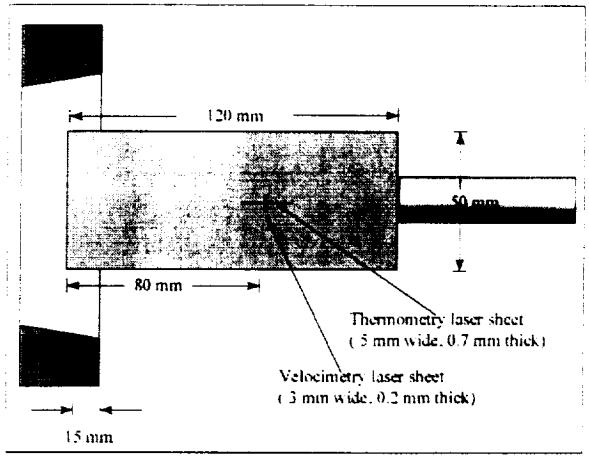

Figure 4 Plan view of the measurement location.

C. Computational Fluid Dynamics

We used the commercial computational fluid dynamics code CFD-FASTRAN™ to predict the streamwise component of velocity.[23] The computational grid was started 10-mm upstream of leading edge of the flat plate. We accounted for the slight flow divergence in the freestream by computing the flow velocity 10-mm in front of the flat plate, assuming a source flow. Then, x- and y-components of velocity were manually input at the inlet boundary. We used Roe's flux differencing scheme with the min-mod flux limiter to achieve second-order spatial accuracy. This Navier-Stokes code uses Sutherland's viscosity model and the ideal gas law to compute the gas density. The ratio of specific heats was assumed to be 1.4. We assumed that the flowfield was laminar and that the Prandtl number was 0.7. The wall temperature was assumed to be 300K. We used approximately 20,000 grid cells in the computation, which converged by 7 orders of magnitude.

Experiment

The experiments were performed on the T2 free-piston shock tunnel at the Australian National University.[24] A schematic of the experiment is shown in Figure 3. The nozzle has a 15 degree full-angle conical geometry with a 5.4-mm diameter throat and a 73 mm exit, resulting in an exit-to-throat area ratio of 183. The nozzle had a throat-to-exit length of 255 mm. The shock-tube was filled with a mixture of 98.9% N_2, 1.1% O_2 to 100 kPa and was at room temperature prior to tunnel operation. This gas mixture was chosen to produce an amount of NO that was substantial enough to produce good fluorescence, but that would minimize the amount of the gases (O_2, O, and NO) that are efficient quenchers. The primary shock speed was 2.4 km/s, which corresponds to a flow enthalpy of 5.8 MJ/kg. The nozzle-reservoir pressure was measured to be 27.5 MPa and reservoir temperature was calculated to be 4591 K using the equilibrium shock tube code ESTC.[25] We used the one-dimensional non-equilibrium code

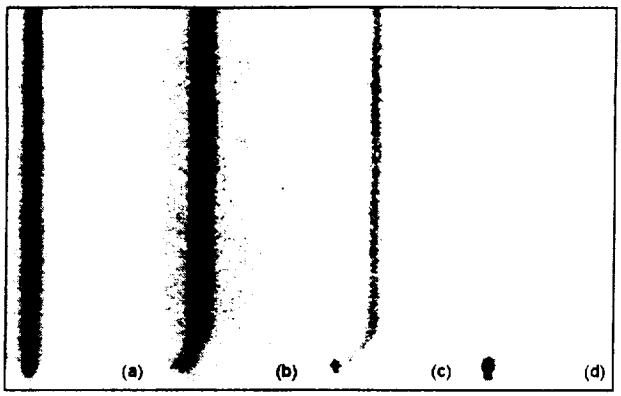

Figure 5 Raw LIF intensities for four delays: 0, 250, 500 and 750 ns for (a)-(d) respectively. Image (a) was obtained in static NO in the test section. Images (b)-(d) were obtained during the shock-tunnel flow.

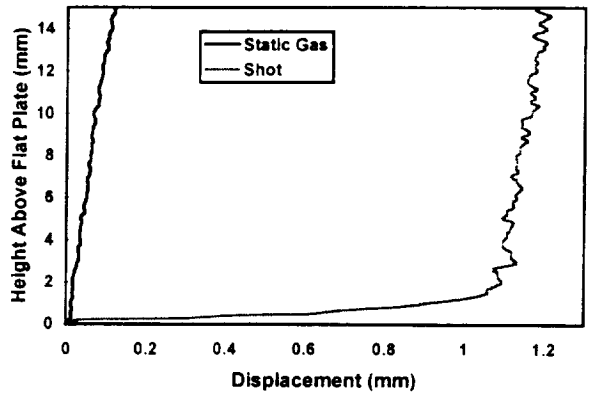

Figure 6 Displacement measurements for shot 725 and for a LIF image taken prior to the shot in static NO.

STUBE to estimate the nozzle-exit conditions (to be used as an inlet condition for CFD-FASTRAN) and to estimate the freestream conditions at the measurement location.[26] At the measurement location, 65 mm downstream of the nozzle exit and 80 mm downstream of the leading edge of the flat plate, STUBE predicts the velocity is 3184±80 m/s, the temperature is 362±25 K and the pressure is 2.4±0.2 kPa, and the Mach number is 8.52±0.05. The estimated gas composition at this location was 98.3% N_2, 1.0% NO, 0.3% O_2, and 0.3% O. The Reynolds number based on the distance from the leading edge of the flat plate is 27,000 whereas the critical Reynolds number for transition to turbulence in a hypersonic flow over a flat plate is 1 million.[27]

During the measurement time, the tunnel recoils 8.0±0.5 mm. After recoil, the tip of the flat plate was located 15±0.5 mm inside the nozzle, corresponding to a distance of 240±0.5 mm from the nozzle throat. As shown in Figure 4, the flat plate was 120 mm long and had a width of 50 mm. It had a sharp leading edge and was mounted from the rear by a sting. As shown in the figure, the laser sheet in the current experiment was oriented perpendicular to the flow and parallel to the line of sight of the camera. Also shown in the figure is the orientation of the laser sheet for the thermometry experiments reported elsewhere.[4] The laser sheet was centred 80±1 mm downstream of the leading edge and was measured to be 0.20±0.05 mm thick.

We frequency-doubled the output of an excimer-pumped dye laser (Lambda Physik, Scanmate II) to obtain 2-mJ, 25-ns pulses at 225 nm, coinciding with the (0,0) vibrational band of the A–X electronic transition of NO. Most of the laser light was formed into a 10-mm wide sheet and was directed into the test section perpendicular to the flow. Approximately 1 mJ was used to form the laser sheet. A small portion of the laser beam was split off and used for wavelength calibration by performing LIF of NO generated by entrainment of nitrogen from room air into an H_2/O_2 welding torch.

Approximately a half hour before each tunnel run, we filled the test section with 1.7% NO in He to a pressure of about 2 kPa. The laser was tuned to the peak of the NO transition. We then obtained a LIF image of the line in the static gas. Next, the test section was evacuated in preparation for a shot. Just prior to each shot we adjusted the laser to the same transition by monitoring LIF in a flame. Immediately before the shot (<5 sec), the tunnel operator stopped the laser via a remote switch next to the firing valve. After the firing valve was opened, the nozzle reservoir pressure transducer detected the shock reflection at the end of the shock tube and the laser fired 350 μs later. This delay was chosen to coincide with the period of steady flow in the shock tube.

An intensified CCD camera (Princeton Instruments, 16-bit CCD, 576 by 384 pixels, 30±3-ns gate duration) captured the fluorescence image at right angles to the laser sheet. The image resolution was 22.4±0.2 pixels per mm. A 2-mm thick UG-5 filter was placed in front of the ICCD camera. This filter allowed the fluorescence above 230 nm to pass into the camera, but cut off most of the elastically scattered laser light and some of the flow luminosity. The filter also blocked resonant fluorescence (A-X (0,0) near 226 nm).

Some light originating from the surface of the flat-plate model is transmitted through the filter. We believe that this could be fluorescence resulting from ablation of the black paint on the model. For the last three shots of the experiment, the paint was removed and the surface was polished which reduced the intensity of the scatter by a factor of 5. We did not want to eliminate this scattered light completely because it serves as an excellent marker for determining the location of the intersection between the laser beam and the flat plate.

We probed the coincidental overlap of four different NO lines: $Q_2(19.5)$ and $Q_1(12.5)$ and their satellite transitions at 44227.71 cm^{-1}. These four transitions were chosen for their appreciable ground-state populations for all temperatures expected in the experiment as well as their strong transition probability which results in strong fluorescence.

Considering the laser energy used, the pulse duration, the beam area, the transition linestrength and an estimate of the flow conditions, we predict that the laser irradiance is 5x the saturation irradiance (I_{sat}) in the freestream. Higher irradiance would not increase the signal intensity much. For this reason, we spread the laser beam out into a sheet 3 mm wide. This increases the signal intensity by a factor of ~15 compared to

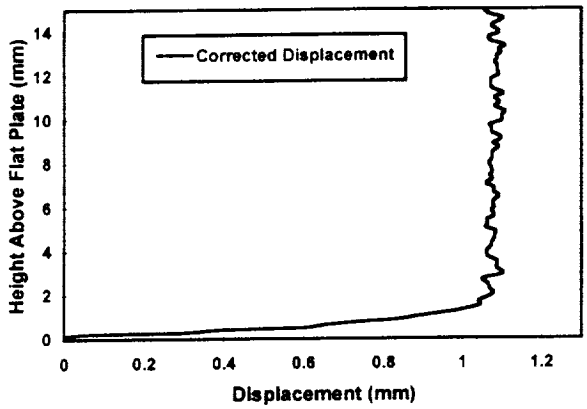

Figure 7 Corrected displacement.

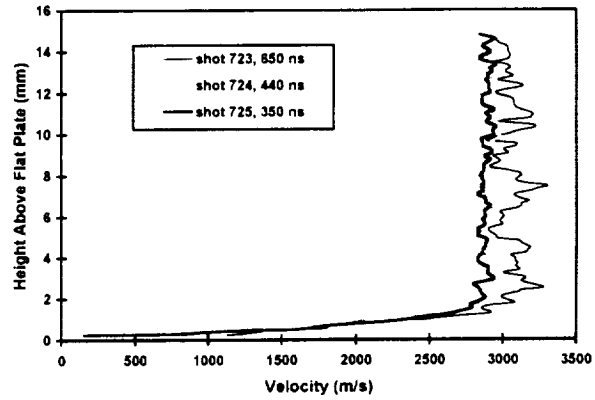

Figure 8 Three typical single-shot velocity measurements.

focussing the beam to a spot 0.2 mm in diameter, because the laser energy is spread out along a line rather than further saturating the transition at a single point. The line was limited to 3 mm because this was a similar length to the camera's depth of field (~2 mm) and a wider sheet would cause the line to blur.

Other approaches were used to increase the signal-to-noise ratio in the raw images. The camera gain was increased to 9.5/10 for some of the longer delays. We used the maximum lens aperture (4.5). The camera was placed as close as possible (about 30 cm) to the measurement location to collect the maximum amount of fluorescence and to provide the highest possible magnification. Also, the camera was oriented slightly above the level of the flat plate so that the full area of the lens would collect fluorescence from the region closest to the plate. These measures were necessary because we estimate that τ_{LIF} = 140 ns. Thus, when τ_d = 750, only 0.5% of the original fluorescence remains! Owing to the precautions described above, good velocity measurements were still obtained at this delay, despite the low signal levels.

Results and Discussion

Figure 5 shows the images obtained at 4 different delays in the experiment. The images are shown side-by-side for clarity. To enable the lower intensity values in the images to be observed, the images display the natural logarithm of the raw data. The zero-delay image was obtained in the static gas in the test section prior to a shot. The 3 other delays were obtained during subsequent tunnel runs. In total, 11 measurements were obtained, using 7 different delays ranging from 0 to 750 ns. The laser enters each image from the top. The flat plate is located at the bottom of each image. A bright spot at the bottom of the images is clearly visible in the three delayed images. This is the previously mentioned scattered light from the flat plate. This point provides a reference mark for zero velocity in each image.

The images clearly show that the freestream flow at the top of each image is fairly uniform. Close to the flat plate, the images show Blasius-like profiles, as expected. Note that the signal-to-noise ratio of the longer delays is significantly worse than the shorter delays. The width of the line in the zero delay image is approximately 6.5 pixels. This is dominated by the width of the laser sheet and blurring caused by the intensifier. The width of the line in the delayed images is approximately 50% larger than the width of the zero-delay image. This increase can be attributed to the finite laser pulse duration and the finite camera gate duration, both of which act to blur the observed line. The width of the line does not appear to increase with delay, τ_d. This implies that thermal diffusion is not a dominant line-broadening mechanism in this experiment.

From these images, we measure the displacement versus height by using the peak-fitting algorithm discussed in the Theory section. Figure 6 shows the displacement measured for shot 725, which had a delay of τ_d = 350 ns. The quality of the data is very good. However, the displacement measured in the freestream is clearly sloped even though we expect a constant freestream velocity. Figure 6 also shows the displacement measured from the fluorescence image obtained in the static gas, prior to the shot. This displacement is also sloped. On each of the 11 pairs of images, these two slopes, caused by slight misalignment of the laser sheet, were approximately the same. We conclude that subtracting the two displacements accurately corrects for misalignment of the laser sheet. Figure 7 shows the corrected displacement resulting from this subtraction.

For most of the shots, the displacement was not able to be accurately determined within 0.3 mm of the wall because of interference from the light scattered by the model. This corresponds to the inner 15% of the boundary layer (based on the measured velocity profile.) The image processing algorithm jumps to this bright spot in the image, producing spurious zero-velocity results near the wall. These bad data points near the wall were examined and omitted by hand. We attempted to crop the bright spot out of the image and then to refit the data, but this gave similarly poor results. A better fitting algorithm may allow the velocity close to the wall to be determined for all images. As mentioned previously, the final three measurements were much less affected by this scatter source. Consequently, these measurements of velocity were obtained slightly closer to the wall (within 0.2 mm).

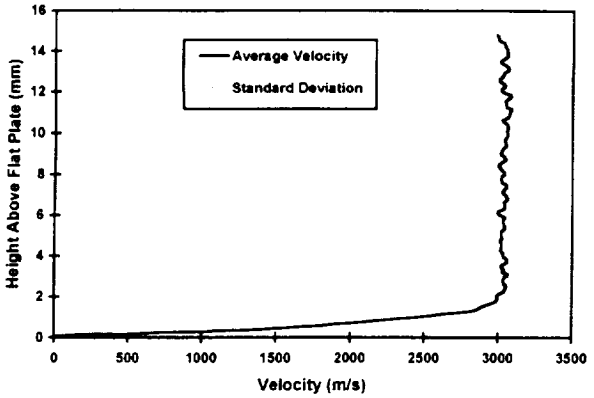

Figure 9 Average and standard deviation of velocity profiles.

Single shot velocity profiles were determined for each shot using Equation 3. Figure 8 shows three of the single-shot velocity measurements. A clear trend observed in the experiment was that longer delays, τ_d, gave noisier velocity profiles. However, the longer delays are not necessarily less accurate, because the measurement uncertainty of the timing decreases with increasing τ_d.

We averaged the 9 single shot velocity profiles obtained from shots where $\tau_d > 0$. We also took the standard deviation of these profiles. The results are shown in Figure 9. The freestream velocity is very uniform and has a value of 3035±60 m/s (uncertainty of ±2%) when averaged from a height of 3 mm to 15 mm above the flat plate. The standard deviation over that same range is 130 m/s. Since 9 measurements are averaged together, the standard error in the mean is 43 m/s. We quote a higher uncertainty than this because of uncertainties associated with systematic errors in the experiment. This measurement uncertainty is a tremendous improvement over previous measurements obtained in the same facility using the spark tracer technique. McIntosh et al[28] measured the freestream velocity to be ~6000±1000 m/s (uncertainty of ±17%) at significantly different flow conditions.

This measured value of the freestream velocity is in agreement with the value of 3184±80 predicted by the STUBE flow code. Considering the simplicity of the STUBE code, we consider this to be satisfactory agreement.

We can also determine the boundary laser thickness from this profile. The boundary layer thickness based on $0.95 \cdot u_\infty$ is 1.4±0.1 mm.

Figure 11 shows a comparison between our measured velocity profile and a CFD-FASTRAN™ simulation of the flowfield, as described in the theory section. Clearly, there is a discrepancy in the freestream. The CFD, which gets its inlet conditions from STUBE, predicts that the freestream velocity is 3185 m/s. The agreement between the CFD and the experiment is within the measurement and calculation uncertainties. The CFD predicts a boundary layer thickness of 1.25 mm, which is ~12% larger than the measurement.

We also used a second method to determine the freestream velocity. We plotted the average of the

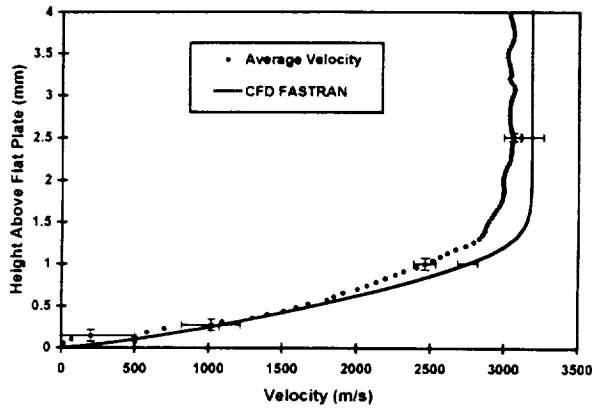

Figure 10 Comparison between measured, average velocity profile and that predicted by CFD-FASTRAN™.

measured displacement from 3 mm to 15 mm above the flat plate for each shot against the total delay, $\tau_d+(\tau_L+\tau_G)/2$. Then a straight line passing through the origin was fit to the data. The resulting graph is shown in Figure 11. Using this method results in a freestream velocity of 3086±60 m/s. This agrees even better with prediction of STUBE than the value obtained by averaging the single-shot velocities.

Some of the measurement points in Figure 11 do not fall exactly on the straight line. Nor does the line fall within the error bars of the measured points, which were determined from statistical variation of the measured displacements between 3 mm and 15 mm above the plate. This discrepancy could be explained by shot-to-shot variation in the tunnel operating conditions. Another explanation is that the magnification of the system could have changed slightly when the camera was re-focused half way though the experiment: the last three measurement points (at τ_d = 350, 440, and 650 ns) all fall below the line.

In determining the measurement uncertainties we considered several different sources of error. Error contributions from most of these sources are shown in Table 1. Significant random errors in the experiment include the ability to measure the shift from the image and the timing jitter in the electronics, particularly in the excimer laser. Note that the uncertainty in measuring the

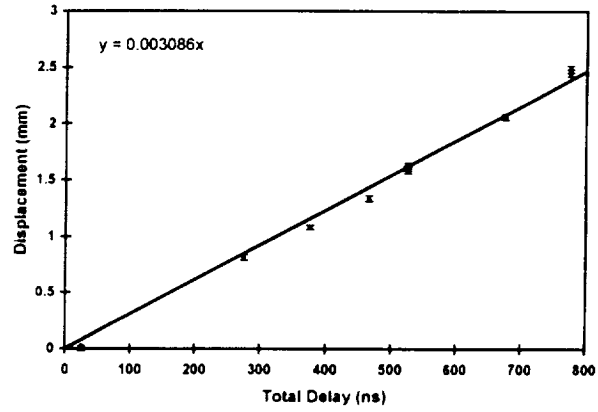

Figure 11 Measurement of average freestream velocity by fitting a straight line through time-of-flight data.

Error Analysis	250 ns	500 ns	750 ns
Random Errors			
Measurement of Shift	1.2	1.8	2.2
Timing Jitter (3 ns)	1.2	0.6	0.4
Total Random Errors	*1.7*	*1.9*	*2.2*
Systematic errors			
Magnification	1.0	1.0	1.0
Laser/Camera Timing (5 ns)	2.0	1.0	0.7
Total Systematic Errors	*2.2*	*1.4*	*1.2*
Overall Uncertainty (%)	*2.8*	*2.4*	*2.5*
Uncertainty at 3000 (m/s)	84	71	76

Table 1 Error analysis computed for τ_d = 250, 500 and 750 ns. Unless otherwise indicated, the numbers are percentages

shift increases with delay because the signal-to-noise of the images decreases whereas the relative uncertainty in the velocity caused by the timing jitter decreases with delay.

Systematic errors in the experiment included the ability to measure the magnification of the optical system and also the timing uncertainties between the laser and camera. This timing uncertainty includes the uncertainty of the laser pulse duration, uncertainty of the camera gate duration, and uncertainty of the absolute time delay between the laser pulse and the camera acquisition. We estimated each of these three timing uncertainties to be ±3 ns. The total measurement uncertainty at a single point in an image for a single shot measurement is then estimated at ±2.5%, though this depends somewhat on delay. Note that the minimum uncertainty occurs for a delay of 500 ns. The uncertainties for averaged freestream velocities were quoted above at ±2% because averaging over many samples reduces the random error, but not the systematic errors.

Another possible source of error that we investigated was that associated with radiative heating of the plate by the laser. This was tested by firing the laser directly at a co-axial thermocouple mounted in the plate and measuring the increase in temperature using the thermocouple. The laser beam occupied the same area as the active area of the thermocouple. The junction for the thermocouple was made by sanding the surface of the thermocouple until it was flush with the model surface. The very small contact area gives the thermocouple a response time of approximately 1 μs. The measured peak temperature was approximately 70K above ambient, decaying exponentially to ambient conditions after 100 microseconds.

The beam used in the velocimetry experiment was much narrower than this beam, but had a similar irradiance. The response time of the thermocouple is still a factor of 100 slower than the pulse duration, so the peak heating may have been greater than measured. However, the response of the flow would be on a similar time scale to the thermocouple. Calculations performed using the analytical method outlined by Haridas[29] show that for a 100 K difference in surface temperature, the velocity profile varies by no more than 1.5% of the freestream velocity in the middle of the boundary layer. The variations near the wall and near the freestream are negligible.

Conclusion

In conclusion, we have demonstrated flow-tagging velocimetry of NO for the first time. We used this method to measure the velocity profile of a laminar boundary layer on a flat plate in a hypersonic flow. The average freestream velocity was measured to be 3035±60 m/s which corresponds to a measurement uncertainty of ±2%.

To our knowledge, these are the first good-quality velocity measurements observed in a laminar hypersonic boundary layer. While agreement between the measurements and CFD isn't perfect, it is much closer than the other known velocity measurements and computations in a laminar, hypersonic boundary layer.[1]

The major advantages of this velocity measurement technique are that it is conceptually simple and easy to interpret. It uses a single laser whereas most flow-tagging methods used two or three lasers. The method is especially convenient for scientists already using PLIF – velocity measurements can be performed with very few modifications to the measurement system. The major disadvantage of the method is that the molecule probed needs to have a long fluorescence lifetime. This limits the applicability of the method to specialised flow facilities, like free piston shock tunnels, where the flow velocity is high and the gas composition can be carefully controlled. Nonetheless, this method should allow a range of velocity measurements in a variety of hypersonic flows of interest to the scientific community.

Acknowledgments

The experiments were carried out at the Australian National University as part of a research program supported by a Faculty Research Grant funded through the Australian National University. We acknowledge the helpful contributions of Ms. Jodie Fox and Mr. Paul Walsh. Also, we acknowledge Dr. Glenn Diskin, NASA Langley Research Center, for providing the image processing routines.

References

[1] Baird, J.P., Lyons, P.R.A. and Gai, S.L., "Measurement of density and velocity profiles in non-equilibrium laminar hypersonic boundary layers in air." In Shock tubes and waves, Proceedings of the 14th International Symposium on shock tubes and shock waves, Archer, R.D., Milton, B.E. (Eds), University of Sydney, New South Wales, Australia, 1983.

[2] Mallinson, S.G., Gai, S.L. and Mudford, N.R., "The boundary layer on a flat plate in hypervelocity flow", The Aeronautical Journal, Vol. 100, April 1996, pp. 135-141.

[3] Palma, P.C., Mallinson, S.G., O'Byrne, S.B., Danehy, P.M. and Hillier, R., "Temperature measurements in a hypersonic boundary layer using planar laser-induced fluorescence," AIAA Journal, Sep 2000, Vol. 38, No. 9, pp 1769-1772.

[4] O'Byrne, S.B., Danehy, P.M, Palma, P.C., Mallinson, S.G., Houwing, A.F.P, "Temperature and velocity measurements in a hypersonic laminar boundary layer". The 23rd International Symposium on Shock Waves, Texas, USA, 2001.
[5] Hart, R.C., Balla, R.J., and Herring, G.C., "Simultaneous velocimetry and thermometry of air using nonresonant heterodyned Laser-Induced Thermal Acoustics", ICASE Report No. 2000-22, May, 2000.
[6] Mosedale, A.D., Elliot, G.S., Carter, C.D., Weaver, W.L., and Beutner, T.J., "On the use of planar Doppler velocimetry," AIAA Paper 98-2809, 1998.
[7] Clancy, P.S., Samimy, M., and Erskine, W.R., "Planar Doppler velocimetry: three-component velocimetry in supersonic jets", AIAA Journal 37, No. 6, 1999, pp. 700-707.
[8] Miles, R.B. and Lempert W. "Two-dimensional measurement of density, velocity, and temperature in turbulent high-speed air flows by UV Rayleigh scattering". Appl. Phys. B. 51, No. 1, 1990, pp. 1-7.
[9] Seasholtz, R.G., "Instantaneous 2D velocity and temperature measurements in high speed flows based on spectrally resolved Rayleigh scattering," AIAA Paper 95-0300, 1995.
[10] Forkey, J.N., Lempert, W.R., Miles, R.B., "Accuracy limits for planar measurements of flow field velocity, temperature and pressure using filtered Rayleigh scattering", Experiments in Fluids, 24, No. 2, 1998, pp. 151-162.
[11] P.M. Danehy, P.Mere, M.J. Gaston, S. O'Byrne, P.C. Palma and A.F.P. Houwing "Fluorescence measurement of the velocity-field produced by the hypersonic separated flow over a cone" AIAA Journal (submitted).
[12] Hiller, B., Hanson, R.K., "Simultaneous planar measurements of velocity and pressure fields in gas flows using laser-induced fluorescence", Appl. Opt., Vol. 27, January, 1988, pp. 33-48.
[13] Paul, P.H., Lee, M.P., Hanson, R.K., "Molecular velocity imaging of supersonic flows using pulsed planar laser-induced fluorescence of NO," Opt. Lett., Vol. 14, May 1989, pp. 417-419.
[14] Allen, M., Davis, S., Kessler, W., Legner, H., McManus, K., Mulhall, P., Parker, T., Sonnenfroh, D., "Velocity field imaging in supersonic reacting flows near atmospheric pressure" AIAA Journal 32(8), 1994, pp. 1676-1682.
[15] Barker, P.F., Thomas, A.M. McIntyre, T.J., and Rubinsztein-Dunlop, H., "Velocimetry and Thermometry of supersonic flow around a cylindrical body," AIAA Journal 36, No. 6, 1998, pp. 1055-1060.
[16] Miles, R.B., Zhou, D., Zhang, B. "Fundamental Turbulence Measurements by RELIEF Flow Tagging", AIAA Journal, MAR 01 1993 v 31 n 3 p. 447.
[17] Orelmann, C., Schulz, C., and Woofrum, J., "NO-flow tagging by photodissociation of NO_2. A new approach for measuring small-scale flow structures", ,Chemical physics letters, v 307 n 1/2 1999, p. 15
[18] Ribarov, L.A., Wehrmeyer, J.A., Batliwala, F., Pitz, R.W., DeBarber, P.A., "Ozone tagging velocimetry using narrowband excimer lasers.", AIAA Journal 37, No. 6, 1999, pp. 708-714
[19] Hiller, B., Booman, R.A., Hassa, C., and Hanson, R.K., "Velocity visualization in gas flows using laser-induced phosphorescence of biacetyl", Rev. Sci. Instrum. 55, December, 1984, pp. 1964.
[20] Seitzman, J.M. and Hanson, R.K., "Planar fluorescence imaging in gases", in 'Instrumentation for flows with combustion', Academic Press Ltd., 1993, pp. 405-465.
[21] Eckbreth, A.C., "Laser disgnostics for combustion temperature and species", 2nd Ed., Gordon and Breach, 1996.
[22] P.H. Paul, J.A. Gray, J.L. Durant Jr., J.W. Thoman Jr, "Collisional quenching corrections for laser-induced fluorescence measurements of NO $A^2\Sigma^+$,"AIAA Journal 32, p. 1670-1675, 1994.
[23] CFD Research Corporation, Cummings Research Park, Huntsville AL 35805, http://www.cfdrc.com/.
[24] Stalker, R.J., "A study of the free-piston shock tunnel," AIAA Journal 5, December 1967, pp. 2160-2165.
[25] McIntosh, M.K., "Computer program for the numerical calculation of frozen equilibrium conditions in shock tunnels," Department of Physics, Faculties, Australian National University, 1968.
[26] Vardavas, I.M., "Modelling reactive gas flows within shock tunnels." Aust. J. Phys. 37, January 1984, pp. 157-177.
[27] He, Y. and Morgan, R.G., "Transition of compressible high enthalpy boundary layer flow over a flat plate", Aeronautical Journal Vol 98, No. 2, 1994, pp. 25-33.
[28] M.K. McIntosh, The Physics of Fluids, Vol. 14, No. 6, June 1971, pp 1100-1102.
[29] Haridas A.K., "Morphology of compressible laminar boundary layers", M.S. thesis, University of Oklahoma, Norman, Oklahoma, 1995.